JOURNAL OF CATALYSIS 117, 155–169 (1989)

Kinetic Simulation of Heterogeneous Catalytic Processes: Ethane Hydrogenolysis over Supported Group VIII Metals

SCOTT A. GODDARD, MICHAEL D. AMIRIDIS, JAMES E. REKOSKE, NELSON CARDONA-MARTINEZ, AND J. A. DUMESIC[1]

Department of Chemical Engineering, University of Wisconsin, Madison, Wisconsin 53706

Received August 23, 1988

A kinetic model for ethane hydrogenolysis over Pt, Pd, Ir, and Co was formulated in terms of essentially two chemical parameters: the strength of bonding between atomic hydrogen and the metal surface and the strength of carbon–metal bonding between hydrocarbon fragments and the surface. These two surface bond strengths were estimated by calorimetric measurements of the heats of H_2 and CO adsorption, combined with bond order conservation calculations. The results of the kinetic simulations suggest that ethane hydrogenolysis over Pt, Pd, Ir, and Co takes place through irreversible C–C rupture of C_2H_4 and C_2H_3 surface species. Hydrogenation of monocarbon CH_y fragments is kinetically insignificant. Dissociative adsorption of hydrogen is an equilibrated process, while dissociative adsorption of ethane is slow and reversible. Finally, the role of kinetic modeling in the formulation, interpretation, and generalization of experimental research in heterogeneous catalysis is discussed.

INTRODUCTION

We have discussed previously (*1*) the concept of using kinetic simulation as a guide to the formulation, interpretation, and generalization of experimental research in heterogeneous catalysis. The basic approach that we have outlined involves (i) the formulation of a reaction mechanism that is based on chemical and spectroscopic evidence, (ii) the estimation of surface thermodynamic properties and rate constants for the intermediates and the elementary steps of the mechanism, and (iii) the simultaneous solution of the surface steady-state equations for reactive adsorbed species, the site balance for the catalyst surface, and the reactor design equations for the reactants and products of the catalytic reaction.

The result of the above procedure is a prediction of the forward and reverse rates for all elementary steps and an estimation of the surface coverages by reactive intermediates under reaction conditions. It is this information that allows one to predict the possible rate determining or kinetically significant elementary steps as well as the most abundant surface species on the catalyst surface. These predictions then suggest experimental studies to test the validity of the kinetic simulations, reactor operating conditions that optimize catalyst performance, and new materials that may be formulated with improved catalytic properties.

Two basic difficulties have prevented this approach from being used widely in heterogeneous catalysis research. The first problem has been in solving the requisite equations for chemically realistic reaction mechanisms. This difficulty, however, can be overcome by the use of modern numerical methods, which have been made readily accessible in a "friendly" manner to researchers due to the rapid development of microcomputers. The second problem,

[1] To whom correspondence should be addressed.

0021-9517/89 $3.00

which is fundamentally more difficult, is that sufficient experimental data are not generally available for the required high precision estimation of surface thermodynamic and kinetic constants, except for selected cases that have been investigated in considerable detail (e.g., *2–5*). Does this mean that kinetic simulation cannot be used as a tool to experimentalists in heterogeneous catalysis research? The present paper addresses this question.

Clearly, without a complete thermodynamic and kinetic description of the surface chemical processes based on direct experimental measurements, one must introduce parameters to conduct kinetic simulations of catalytic reactions. It is important, however, that these parameters have physical significance. Examples of such parameters include surface bond energies, sticking coefficients, and preexponential factors for surface reactions. In general, the kinetic simulation should not make a priori assumptions about rate determining steps or most abundant surface intermediates; therefore, estimates of rate constants for all steps of the reaction mechanism must be made using physically meaningful parameters in the microkinetic model. With reasonably good estimates for these kinetic parameters, it is then possible to predict which steps of the mechanism are kinetically significant or rate determining, and which surface species are most abundant.

While the above process may apparently involve a large number of kinetic parameters, it is important to note that only a small number of these need to be known with precision. Specifically, most of the kinetic parameters are used only to decide the relative importance of the various steps of the reaction mechanism, and since many steps in the mechanism are generally determined to be kinetically insignificant (e.g., *6*), many of the apparent kinetic parameters are not important in the microkinetic model. Accordingly, the parameters of the kinetically significant steps are the ones that are critical, and these are the parameters that the designer must manipulate to produce new catalytic materials.

In the present paper, we apply the aforementioned approach in a preliminary fashion to ethane hydrogenolysis over silica-supported Pt, Pd, Ir, and Co. This reaction has been studied by many authors, since ethane is the simplest hydrocarbon that can undergo cracking of the C–C bond. Perhaps the most extensive investigation of this reaction has been made by Sinfelt (*7, 8*), who studied ethane hydrogenolysis over all of the Group VIII metals and Re.

Although much studied, the mechanistic details of ethane hydrogenolysis are still a source of disagreement in the literature. Previous kinetic analyses of the reaction have utilized various assumptions about rate determining steps and most abundant surface intermediates to deduce the chemical nature of the dicarbon species which is the precursor to C–C bond cleavage. While these models have been successful in closely matching experimental kinetic parameters, they still require a priori assumptions about surface processes. The objective of the present work was to determine if the kinetics of this reaction could be described by a kinetic model using only a limited number of physically meaningful parameters. In addition, we wanted to test whether such a model could explain the significant amount of chemical information in the literature regarding the rate limiting steps, the most abundant surface intermediates, and the carbon/hydrogen surface stoichiometry. For this purpose we have used essentially two parameters in our kinetic simulation: the strength of atomic hydrogen bonded to the surface, EH, and the strength of carbon–metal single bonds between the hydrocarbon fragments and the surface, EC.

Perhaps most importantly, we require the values of EH and EC to be consistent with experimental calorimetric measurements. Accordingly, we have measured in this study the heats of adsorption of H_2 and CO on silica-supported metals using microcalo-

rimetry. The values of EH can be obtained directly from the heat of hydrogen adsorption, since the adsorption of one molecule of H_2 involves the rupture of the H–H bond (104 kcal/mol) and the formation of two hydrogen–metal bonds. The measurement of EC, however, is not as direct, since a variety of adsorbed species may form when ethane is exposed to a metal surface; thus, the interpretation of the calorimetric measurement is ambiguous.

To obtain an estimate of EC from calorimetric measurements, we employ the bond order conservation theory of Shustorovich (*9*). The key parameter of this theory is the strength of the bond between a single carbon atom and the surface. The value of this parameter can be estimated by calorimetric measurements of the heat of CO adsorption on the metal surface.

EXPERIMENTAL/RESULTS

The heats of adsorption of H_2 and CO on silica-supported Pt, Ir, and Co were measured in our laboratory, while the corresponding heats on Pd were reported by Chou and Vannice (*10, 11*). The catalysts used for the calorimetric measurements were prepared and treated in a manner similar to that described by Sinfelt in his work on these three metals (*12–14*). Briefly, the silica support (Cabosil HS5, Cabot Corp.) was impregnated by an aqueous solution of the metal salt: $H_2PtCl_6 \cdot (H_2O)_6$ (Strem Chemicals), $IrCl_3 \cdot 3H_2O$, or $Co(NO_3)_2 \cdot 6H_2O$ (Aldrich Chemicals). The metal content of the catalysts was 1% for Pt/SiO_2 and 10% for Ir/SiO_2 and Co/SiO_2. The catalysts were dried overnight at 383 K and then reduced in flowing hydrogen (Airco), which was purified with a Deoxo unit (Engelhard Industries) and a molecular sieve at 77 K. The reduction treatment was for 1 h at 773 K (preceded by a 24-h treatment in O_2 at 773 K) for Pt/SiO_2, 2 h at 673 K for Ir/SiO_2, and 5 h at 673 K for Co/SiO_2.

A detailed description of the microcalorimeter is given elsewhere (*15*). Briefly, it consists of a Setaram C80 heat flow microcalorimeter of the Calvet type with a sensitivity of 1 mJ, connected to a stainless-steel, calibrated, volumetric system. Isotherm pressures are measured by means of a MKS Baratron Model 398 capacitance manometer. The temperatures of the cells and dosing volumes are measured using a pair of precision platinum resistance temperature devices.

During the experiments, about 1 g of catalyst was loaded in the sample cell and subsequently degassed at 423–623 K for 2–4 h. Reduction treatments were then carried out and the sample was cooled under dynamic vacuum to 308 K. The cells and the sample were evacuated overnight to allow the system to approach thermal equilibrium.

To start the adsorption of hydrogen or carbon monoxide, a known amount of gas was placed in a calibrated dosing volume and then dosed into the sample and the reference calorimeter cells. The heat released upon dosing the gas was detected by the calorimeter and recorded in an Apple IIe computer. Subsequently, the area under the thermogram was calculated, along with the amount of gas adsorbed and the differential heat of adsorption per mole of adsorbed gas.

In Figs. 1–3, the differential heats of hydrogen and carbon monoxide adsorption are plotted as functions of surface coverage. Table 1 summarizes the calorimetric results of the metal–hydrogen and metal–carbon bond strengths for the three metals

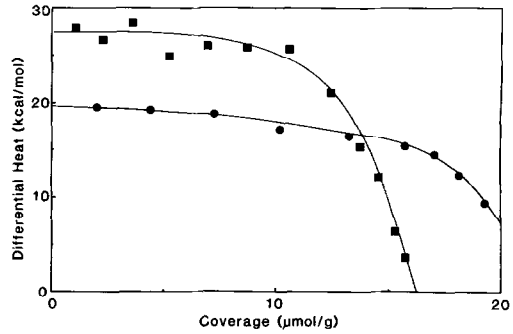

FIG. 1. Differential heats of adsorption of H_2 and CO on Pt/SiO_2 at 308 K; (●) H_2, (■) CO.

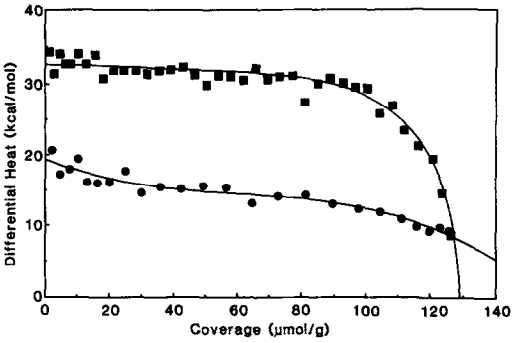

FIG. 2. Differential heats of adsorption of H_2 and CO on Ir/SiO_2 at 308 K; (●) H_2, (■) CO.

studied plus the results for Pd by Chou and Vannice.

The heat of adsorption for hydrogen used in the calculation of EH corresponds to coverages between 20 and 80% of a monolayer. Lower coverages were assumed in the calculation of EC from the heat of carbon monoxide adsorption, since the surface coverage by hydrocarbon species during ethane hydrogenolysis is believed to be low (*7, 16, 17*). The results of our kinetic simulations satisfied both assumptions, since the hydrogen coverage varies from 35 to 75% and hydrocarbon coverage is always less than 2%.

The heats of adsorption for hydrogen and carbon monoxide on Pt, Ir, and Co metals have been reported previously in the literature (*18–24*), and these are in general agreement with our measurements.

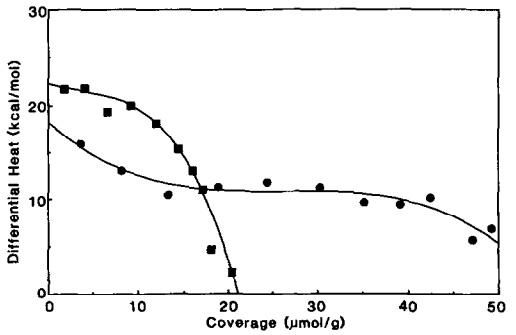

FIG. 3. Differential heats of adsorption of H_2 and CO on Co/SiO_2 at 308 K; (●) H_2, (■) CO.

TABLE 1

Heats of Adsorption of Hydrogen and Carbon Monoxide on Pt, Pd, Ir, and Co

Catalyst	Range for H_2 heat of adsorption (kcal mol^{-1})	Range for CO heat of adsorption (kcal mol^{-1})
Pt/SiO_2	14.8–20.3	26.3–29.9
Pd/SiO_2[a]	14–16	20–25
Ir/SiO_2	11.9–17.2	31.1–35.4
Co/SiO_2	9.6–15.5	20.3–23.4

[a] Results from Refs. (*10, 11*).

GENERAL MECHANISM FOR ETHANE HYDROGENOLYSIS

Several different mechanisms have been proposed in the literature for ethane hydrogenolysis over supported metals (*7, 8, 16, 25–30*). Although there is disagreement on the details of individual steps, there is general agreement on the nature and the sequence of these steps. Qualitatively, the general aspects of these mechanisms can be summarized as follows:

a. hydrogen is adsorbed on the surface in atomic form;

b. ethane is adsorbed dissociatively, undergoing cleavage of a C–H bond;

c. further dehydrogenation of the C_2H_5 species occurs, accompanied by the creation of additional bonds between the C_2H_x species and the metal surface;

d. the C–C bond breaks and CH_y species are produced; and finally

e. hydrogenation of the CH_y species takes place, followed by the desorption of methane.

Following the aforementioned ideas, a possible general mechanism for ethane hydrogenolysis over supported metals is suggested below.

$$H_2 + 2^* \rightleftarrows 2H^* \quad (1)$$

$$C_2H_6 + 2^* \rightleftarrows CH_3\text{–}\underset{|}{\underset{*}{CH_2}} + H^* \quad (2)$$

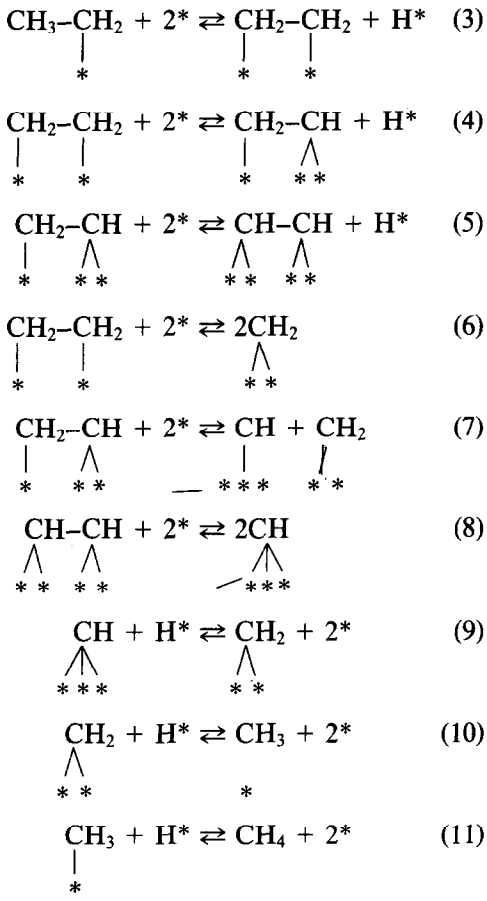

(3) (4) (5) (6) (7) (8) (9) (10) (11)

It should be emphasized that while there is no general consensus regarding the manner in which the C_2H_x species are attached to the surface (*8, 25, 26, 31*), the extent of dehydrogenation before the C–C bond is cleaved, and the nature of the multiple bonding between the C_2H_x species and the metal surface (*25, 26*), the mechanism above is believed to represent the basic surface chemistry involved in ethane hydrogenolysis. The strength of this mechanism is its generality, since it allows a variety of hydrocarbon species to be formed and it does not specify which C_2H_x species is involved in the primary pathway for cleavage of the C–C bond. In particular, the proposed mechanism can be separated into the following three independent routes: Route A (steps 1–3, 6, 10, 11), Route B (steps 1–4, 7, 9–11), and Route C (steps 1–5, 8–11). We also examined the possibility of an earlier cleavage (through a C_2H_5 intermediate), but found that this step did not show significant activity. A deeper dehydrogenation cleavage (through a C_2H intermediate) was considered improbable, since the existing deep dehydrogenation route (C) was quite inactive. Furthermore, we do not make any assumptions about the existence of rate determining steps or most abundant surface species, and we allow all steps to be reversible. Finally, it is important to note that while the above mechanism is not necessarily complete or correct in detail, it agrees with most of the existing literature. The general scheme is similar to mechanisms proposed by Paál and Tétényi (*25*), Tétényi *et al.* (*26*), and Gudkov *et al.* (*29*), differing from them in only minor details. It also agrees with the basic concepts underlying the simpler mechanisms proposed by Sinfelt (*7, 8*), Boudart (*16*), and Frennet and co-workers (*28, 30*).

FORMULATION OF KINETIC MODEL

Rate constants for each elementary step were estimated by the use of Arrhenius expressions $k_i = A_i \exp(-E_{A_i}/RT)$. Order of magnitude estimates were made for the preexponential factors (A_i) using transition state theory. The preexponential factors for the adsorption of gaseous hydrogen and ethane were estimated to be 10^5 and 10^4 $Torr^{-1}$ s^{-1}, respectively, assuming that the surface species were immobile. The preexponential factors for reactions involving only adsorbed species or for desorption processes were estimated to be 10^{13} s^{-1}. When these rate constants are multiplied by gaseous pressures (in Torr) and by fractional surface coverages, the calculated rates are expressed in turnover frequencies (molecules reacted per site per second).

Activation energies (E_{A_i}) were estimated in the following manner. First, the heats of formation of the various intermediates were estimated, assuming that they were formed in the gas phase. During this process known or estimated bond dissociation energies and

heats of formation of gaseous molecules and radicals were used. The estimated gaseous heats of formation were converted to surface heats of formation by the use of the metal–carbon (EC) and metal–hydrogen (EH) bond strengths. Then, the heat of each individual reaction was calculated by the use of the heats of formation of the species involved. Finally, the activation energies were related to the heats of reaction using the Polanyi expression (6):

$$E_{A_i} = E_0 + \alpha H_i. \qquad (12)$$

The parameters E_0 and α depend on the type of reaction, but are independent of the catalyst used. This expression can be viewed either as a simplified linear free-energy relation or as the first two terms of a Taylor expansion of the function which relates the activation energy to the enthalpy of reaction.

The values of EH used in the kinetic simulations were determined calorimetrically from the relation

$$\mathrm{EH} = \frac{D_{H_2} - Q_{H_2}}{2}, \qquad (13)$$

where D_{H_2} is the gas phase dissociation energy of H_2 (104 kcal mol^{-1}) and Q_{H_2} is the heat of adsorption of H_2 on the metal surface. These values of EH are listed in Table 2. Bond order conservation (BOC) calculations were employed to provide initial estimates of EC and the Polanyi parameters, E_0 and α, for each step of the mechanism, as described below.

Briefly, the BOC theory of Shustorovich (*9*) involves the use of a Morse potential to determine the total energy E of a two-center metal-adsorbate (M–A) interaction. The two center M–A bond order x

$$x = \exp[-(r - r_0)/a] \qquad (14)$$

is an exponential function of the M–A distance r. The two-center Morse potential, including only linear and quadratic terms in x, is

$$E(x) = -Q(x) = -Q_0(2x - x^2), \qquad (15)$$

TABLE 2

Metal–Hydrogen and Metal–Carbon Bond Energies Determined from Calorimetry and Bond Order Conservation Calculations for Pt, Pd, Ir, and CO

Catalyst	Hydrogen: Range for EH (kcal mol^{-1})	EH value used in simulations (kcal mol^{-1})
Pt/SiO_2	59.4–62.2	61.0
Pd/SiO_2	59.0–60.0	60.8
Ir/SiO_2	58.0–60.6	58.7
Co/SiO_2	56.8–59.8	55.5

Catalyst	Carbon monoxide: Range for EC (kcal mol^{-1})		EC value used simulations (kcal mol^{-1})
	Using Eq. (15)	Using Eqs. (17) and (18)	
Ir/SiO_2	50.5–66.4	46.4–50.1	49.0
Pt/SiO_2	49.6–59.4	42.1–45.4	47.6
Pd/SiO_2	39.5–51.0	36.0–40.9	47.4
Co/SiO_2	37.6–49.4	36.3–39.4	47.2

where Q_0 is the M–A equilibrium bond energy. When the bond order x is equal to 1 (at the equilibrium distance r_0), the total energy $E(x)$ is a minimum. Since the minimum occurs at $x = 1$, the conservation of $x = 1$ is assumed for multiple-center M_n–A interactions, which are treated as pairwise additives.

When the M_n–A interactions are limited to the n nearest-neighbor metal atoms, the value of the maximum M–A bond energy is given by the equation

$$Q_n = Q_0(2 - 1/n), \qquad (16)$$

where Q_0 is the maximum M–A bond energy in the on-top ($n = 1$) site. One of the conclusions of BOC theory is that adatoms will occupy the highest symmetry sites in hollow depressions. This preference changes to sites of lower coordination, however, if the adatoms are small or steric constraints exist.

According to Shustorovich, the strength of the bond formed between an adsorbed atom (such as C) and the metal surface can be calculated by the use of Eq. (16) with $n = 4$ for C_{4v} symmetry. This leads to the equation

$$EC = \frac{D_m(2 - \frac{1}{4})}{4}, \qquad (17)$$

where D_m is the maximum M–A bond energy in the on-top position. The relationship among D_m, the heat of adsorption of CO, Q_{CO}, and the gas phase dissociation energy D_{CO} (256 kcal/mol for CO) is described by Eq. (18):

$$Q_{CO} \approx \frac{D_m^2}{D_{CO} + D_m}. \qquad (18)$$

Equations (17) and (18), combined with the calorimetric data for Q_{CO}, provide a first estimate for the EC parameter for each metal, which have been shown in Table 2.

Another method for determining the EC bond strength of each surface species is to use bond order conservation around a single carbon atom of the hydrocarbon fragment, and from this determine the metal–carbon bond order. When this value is used in Eq. (15), the energy of the EC bond can be calculated. Values of EC using this method are also listed in Table 2. It is important to note that the values of EC determined in this manner for the hydrocarbon surface species of the mechanism varied by about 10%, providing some justification for using a single value of EC for all surface species on a given metal surface.

The ranges for EC determined from BOC calculations were only used as initial estimates. Although some of the EC values used in the simulations do not lie within these ranges, the strengths of the EC bonds for the four metals were kept in the same order as estimated by calorimetry and BOC theory.

The Polanyi parameters E_0 and α were also estimated by the use of BOC theory. First, the energies for all the stable intermediates in the reaction mechanism were calculated using the aforementioned equations. Using the energies of the gas phase molecules and the surface intermediates, the change in enthalpy was determined for each elementary step. The activation energies of the individual steps were then calculated in a similar manner. The energy differences in this case, however, were calculated for each step between the reactant and a transition state complex. The transition state was analogous to the complex proposed by Shustorovich (*9*) for the dissociation of a diatomic molecule on a metal surface.

Finally, α was calculated for each step by rearranging Eq. (12) in the manner

$$\alpha = \frac{\Delta E_A}{\Delta(\Delta H)} = \frac{E_{A2} - E_{A1}}{\Delta H_2 - \Delta H_1}, \qquad (19)$$

where E_{A1} and ΔH_1 were determined from bond order conservations by varying D_m by ± 10 kcal mol^{-1}. The Polanyi constants E_0 were then calculated by the use of Eq. (12). These calculations showed that some reaction steps had nearly the same value of α. These steps were grouped together and values for α were assigned as follows: steps 1–5, $\alpha = 0.8$; steps 6–8, $\alpha = 0.5$; and steps 9–11, $\alpha = 0.2$. These constants were assigned at the beginning of the simulation and were not allowed to vary thereafter.

To decrease the number of parameters used in the kinetic simulation, the 11 possible values of E_0 were grouped into 4 families according to the nature of the elementary steps. Group A was hydrogen adsorption (step 1), group B was dehydrogenation and hydrogenation (steps 3, 4, 5, 9, 10, and 11), group C was C–C bond breaking (steps, 6, 7, and 8), and group D was ethane adsorption (step 2).

IMPLEMENTATION OF KINETIC MODEL

The first effort of our kinetic modeling study, as has been mentioned, was to simulate the kinetic data collected by Sinfelt and co-workers for Pt, Pd, Ir, and Co (*7, 8*). Turnover frequencies at the conditions where the original experiments were per-

formed were first calculated using values for the activation energy, preexponential factors, and reaction orders measured by Sinfelt. An optimization process was then undertaken in the following manner to determine the parameters that provided results which matched the experimental kinetics. First, we set the value of EH to be within or near the range determined calorimetrically. Then, we varied the value of EC within or slightly outside the range estimated by bond order conservation. Finally, we searched for a set of constant values of E_0 (within about 5 kcal/mol of those values estimated by BOC theory) that allowed the kinetic model to fit the reaction orders, activation energy, and turnover frequencies over all four metals. It should be noted that the turnover frequencies over these four metals vary by five orders of magnitude. In view of the experimental difficulty in determining the number of active sites on a catalyst surface and the 10^5 range of catalytic activities for these metals, we required the kinetic model to predict the true turnover frequency within only a factor of 20. In addition, we did not adjust any of the preexponential factors during our attempts to match Sinfelt's experimental data with our kinetic model.

The final values of EH and EC that were used in our kinetic simulations are shown in Table 2. The corresponding values of E_0 for groups A, B, C, and D were 16, 24, 28, and 23 kcal/mol, respectively, and these varied by no more than 1 kcal/mol over the four metals studied. The overall activation energy, E_A, and the reaction orders with respect to ethane, n, and hydrogen, m, obtained from the model, together with those obtained by Sinfelt are reported in Table 3. The overall agreement is excellent.

TABLE 3

Experimental and Predicted Activation Energies and Reaction Orders[a] for Ethane Hydrogenolysis

Metal	E_A Cal. (kcal mol^{-1})	E_A Exp. (kcal mol^{-1})	$n_{Cal.}$	$n_{Exp.}$	$m_{Cal.}$	$m_{Exp.}$
Pt	55.3	54.0	1.0	0.9	−2.5	−2.5
Pd	56.7	58.0	1.0	0.9	−2.6	−2.5
Ir	35.4	36.0	1.0	0.7	−1.5	−1.6
Co	28.3	30.0	1.0	1.0	−0.9	−0.8

[a] $r = kP^n_{C_2H_6} P^m_{H_2}$

GENERAL DISCUSSION OF RESULTS

The number of hydrogen atoms in the C_2H_x species which is involved in the C–C bond rupture has been a subject of debate in the literature. Different values have been proposed for the different metals which, in the case of Pt for example, range from 0 (*7, 8*) to 5 (*29*). It is interesting to examine what our kinetic model predicts.

As mentioned earlier, the proposed mechanism can be separated into three independent routes, each accounting for a different degree of dehydrogenation. The percentage of the overall reaction proceeding through each route was determined by the ratio of the net rate of step i to the overall net rate, with step i being the characteristic C–C bond breaking step of the route (i.e., step 6, 7, or 8 for Routes A, B or C, respectively). Route C was not used by any of the four metals over the range of experimental conditions investigated by Sinfelt. In general, the percentage of the overall reaction proceeding through Routes A and B depends on the catalyst used, the temperature, and the partial pressures of the reactants. As an example, at a common set of reaction conditions (478 K, 152 Torr of hydrogen and 22.8 Torr of ethane), Route A is more important for Pt and Pd, while Route B dominates for Ir and Co.

In the range examined (7.6 to 76 Torr), it appears that the partial pressure of ethane does not influence the routes through which the reaction occurs. On the contrary, the partial pressure of hydrogen appears to have a significant effect over the range examined (76–300 Torr). As expected, higher hydrogen partial pressures favor the routes which involve the less dehydrogenated hydrocarbon species. Consequently, when Routes A and B compete, the percentage of the overall reaction proceeding through the former route increases as the hydrogen

pressure increases. Temperature has a significant influence on the routes through which the reaction occurs. As the temperature increases, Routes B and C become more favored at the expense of Route A.

Figures 4–7 are representative, qualitative diagrams of the forward and reverse rates for the individual steps of the primary hydrogenolysis routes for the different metals studied. The following qualitative generalizations can be drawn from the kinetic modeling results:

a. steps 6 and 7 (the breaking of the C–C bond) are irreversible for all of the catalysts studied;

b. steps 1 and 4 (adsorption of hydrogen and dehydrogenation to C_2H_3) are close to equilibrium;

c. step 3 (the first dehydrogenation step) is close to equilibrium for Pt and Pd, but slow and reversible for Ir and Co;

d. step 2 (adsorption of ethane) is slow and reversible for all of the catalysts studied; and

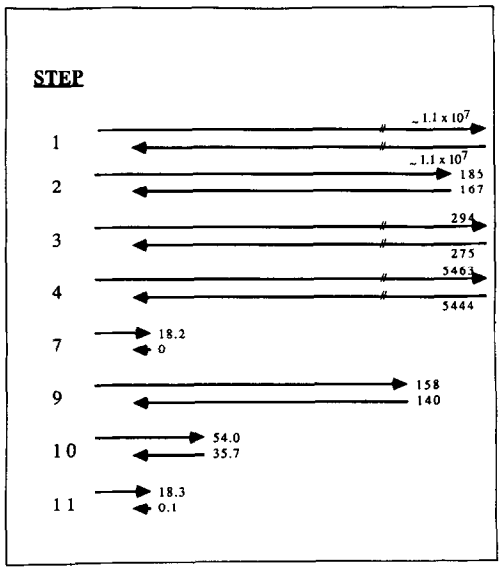

FIG. 5. Schematic diagram of the relative rates (10^{-3} s^{-1}) of elementary steps for ethane hydrogenolysis (Route B) over Pd/SiO_2 at 630 K, P_{H_2} = 152 Torr and $P_{C_2H_6}$ = 22.8 Torr. Forward and reverse rates for each step have been divided by the stoichiometric number of that step.

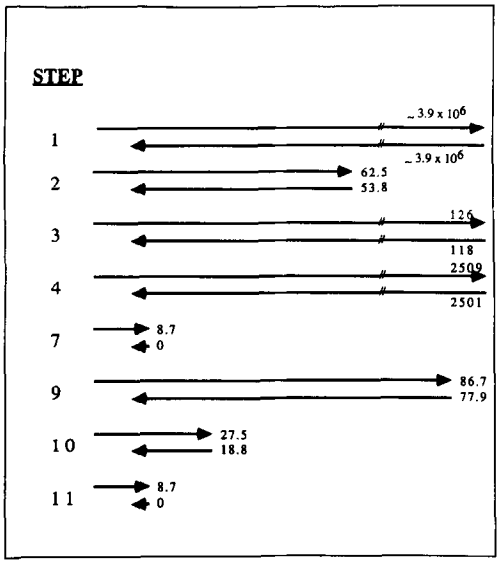

FIG. 4. Schematic diagram of the relative rates (10^{-3} s^{-1}) of elementary steps for ethane hydrogenolysis (Route B) over Pt/SiO_2 at 630 K, P_{H_2} = 152 Torr and $P_{C_2H_6}$ = 22.8 Torr. Forward and reverse rates for each step have been divided by the stoichiometric number of that step.

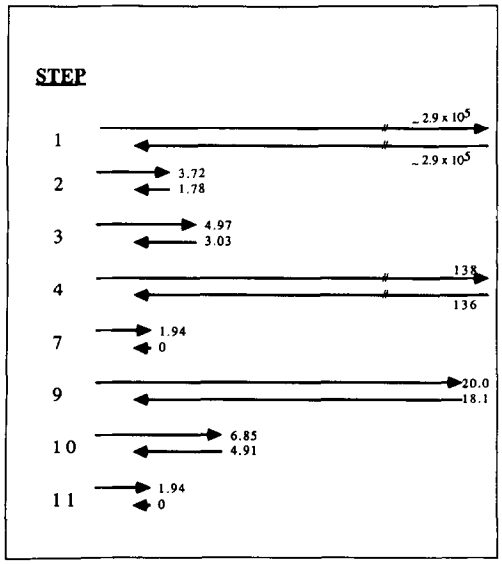

FIG. 6. Schematic diagram of the relative rates (10^{-3} s^{-1}) of elementary steps for ethane hydrogenolysis (Route B) over Ir/SiO_2 at 480 K, P_{H_2} = 152 Torr and $P_{C_2H_6}$ = 22.8 Torr. Forward and reverse rates for each step have been divided by the stoichiometric number of that step.

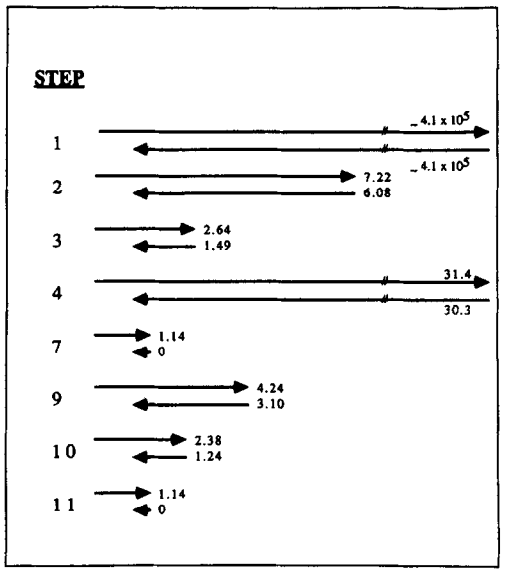

FIG. 7. Schematic diagram of the relative rates (10^{-3} s^{-1}) of elementary steps for ethane hydrogenolysis (Route B) over Co/SiO_2 at 490 K, P_{H_2} = 152 Torr and $P_{C_2H_6}$ = 22.8 Torr. Forward and reverse rates for each step have been divided by the stoichiometric number of that step.

e. steps 9, 10, and 11 (hydrogenation of C_1 fragments and desorption of CH_4) are kinetically insignificant.

COMPARISON OF KINETIC MODEL WITH EXPERIMENTAL DATA

In this section, we will compare assumptions, conclusions, and experimental results from the literature to the predictions of the present kinetic model. The first part will be a comparison of general results, while the second part will examine specific experimental data from studies on individual metals.

The work of Sinfelt (*7, 8*) has been one of the most complete in the area of ethane hydrogenolysis. A table comparing his experimental results with the predictions of the proposed model has already been given. Sinfelt concluded that hydrogen is in excess on the catalytic surface and supported the assumption originally made by Cimino *et al.* (*32*) that the concentration of the intermediate C_2H_x in the reaction sequence decreases with increasing hydrogen pressure. Both concepts are predicted by the proposed model.

A number of hypotheses were made by Sinfelt regarding the rate of individual steps. It was assumed, for example, that hydrogen adsorption was an equilibrium process, in agreement with the present model. It was also assumed by Sinfelt that the carbon–carbon bond rupture is rate determining. This step is indeed predicted to be irreversible and kinetically significant for all four metals.

Finally, according to the work of Sinfelt on cobalt, equilibrium is effectively maintained at low temperatures between adsorbed C_2H_x and gas phase ethane, while the chemisorption of ethane at high temperatures is effectively irreversible. The present model predicts that the ratios r_2/r_{-2} and r_3/r_{-3}, expressing the degree of irreversibility for ethane adsorption and subsequent dehydrogenation, increase with increasing temperature. For example, the ratio r_2/r_{-2} for Co was found to be equal to 1.0 at 350 K, and it increased to 1.19 and 1.51 as the temperature increased to 492 and 532 K, respectively. Consequently, the proposed model agrees with the observation of Sinfelt.

Frennet *et al.* (*33*) used deuterium tracing and transient kinetic methods to study ethane hydrogenolysis over a Rh film. They were able to determine that the coverage of hydrocarbon residues was less than 2% of the hydrogen chemisorption sites, in agreement with our model. Furthermore, they studied the forward and reverse rates of the different elementary steps. They concluded that all C_2H_x species are reversibly chemisorbed, the breaking of the C–C bond is reversible, a unique rate determining step does not exist (i.e., all rates are within an order of magnitude), and the only irreversible step is the desorption of methane. Although the catalytic behavior of rhodium has not been simulated in this study, the present model shows indeed the absence of

a rate determining step and the irreversibility of methane desorption for Rh. In addition, steps 2, 3, and 4 (ethane adsorption and the subsequent dehydrogenations) are predicted to be reversible in agreement with the experimental results. Finally, although for the catalysts and conditions studied the C–C bond breaking step was predicted to be irreversible, we have observed reversibility for this step using different bond energies.

Boudart (*16*) analyzed ethane hydrogenolysis according to a two-step reaction mechanism on a nonuniform surface. It was assumed that C_2H_x species are the most abundant intermediates among the carbon-containing species, which the present kinetic model predicts in almost every case. It was also assumed that gas phase and adsorbed hydrogen are in equilibrium, while the hydrocarbon is adsorbed irreversibly to give the C_2H_x species which undergoes C–C bond cleavage. The present model agrees with the former assumption; however, it predicts that the adsorption of ethane is slow and reversible for the metals examined.

Tétényi *et al.* (*26*) have compared adsorption and H–D exchange data for CH_4 and C_2H_6 with hydrogenolysis on several metal blacks (Co, Ni, Rh, Pd, Ir, and Pt). Their results supported the possibility of a 1,2-diadsorbed ethane species and the idea of a multiply bonded C_1 species (either CH_2M or CH_2M_2). Both ideas agree with the present model. By comparing the hydrogenolysis and H–D exchange rates, these authors concluded that hydrocarbon adsorption is not rate determining. Instead, they proposed the rupture of the C–C bond as the rate determining step. The present model is consistent with these two qualitative observations.

Guczi *et al.* (*28*) reported a maximum in the rate of hydrogenolysis as the hydrogen pressure increased. The present kinetic model shows this same behavior. Furthermore, they suggested that the maximum should shift toward higher pressures as the reaction temperature increases. In agreement with this observation, the present model predicts, for example, that as the reaction temperature increases from 627 to 647 K for Pd, the maximum rate shifts from 7.0 to 9.5 Torr.

Two different routes were proposed by Guczi *et al.* for ethane hydrogenolysis, involving different degrees of dehydrogenation of the C_2H_x-surface species which undergoes C–C bond scission. In agreement with the present model, it was suggested that when the hydrocarbon-to-hydrogen ratio increased, more deeply dehydrogenated species were involved in the mechanism. They also suggested that when deep dehydrogenation occurs, hydrocarbon species predominate on the surface. While the present model does show an increase in hydrocarbon coverage when the reaction proceeds through deeper dehydrogenation routes, it always remains less than the surface coverage of hydrogen.

Ethane hydrogenolysis on Pt/SiO_2 and $PtFe/SiO_2$ was studied by Gudkov and coworkers (*29*) over a wide range of reactant concentrations. According to them, if hydrogen is in excess, then C–C bond rupture occurs mostly through the C_2H_5 intermediate, whereas if ethane is in excess, it occurs mostly through the more dehydrogenated intermediate C_2H_2. Using the same temperatures and pressures, our model predicts that for excess hydrogen, most of the reaction proceeds through the C_2H_4 intermediate, with the remainder going through C_2H_3. For excess ethane, the reaction proceeds almost exclusively through the more dehydrogenated C_2H_3. In addition, Gudkov *et al.* determined the overall activation energy of the reaction to be 46.4 kcal mol^{-1} in excess hydrogen and 23.4 kcal mol^{-1} in excess ethane. Activation energies by our model were 57.6 and 19.1 kcal mol^{-1}, respectively. However, by lowering the EH and EC bond energies by 2.0 kcal mol^{-1} to account for possible differences in the catalysts studied by Sinfelt and Gudkov *et al.*, our model predicts activation energies of

50.0 kcal mol^{-1} for excess hydrogen and 25.2 kcal mol^{-1} for excess ethane.

Sárkány *et al.* (*34*) showed that ethane hydrogenolysis over Pt was not inhibited by methane, supporting the conclusion that methane formation and desorption proceed rapidly. In agreement, our results show that the hydrogenation steps (9 and 10) and methane desorption (step 11) are kinetically insignificant, and the rate is independent of the methane pressure.

The adsorption of ethane on a hydrogen-covered platinum film was studied by Anderson and Baker (*35*). By observing the amount of hydrogen released, they calculated that the H/C ratio of the adsorbed ethane residue was between 0.8 and 1.8. Under the same conditions, our model, taking into account all of the adsorbed hydrocarbon intermediates, predicts a value for H/C of 1.0.

Foger and Anderson (*36*) investigated ethane hydrogenolysis over a series of dispersed iridium catalysts. The reaction occurred with an activation energy near 42 kcal mol^{-1}, and the rate was proportional to $P_{HC}^{1}P_{H_2}^{-2.9}$. Using their conditions, our model predicts an activation energy of 42 kcal mol^{-1} and rates proportional to $P_{HC}^{1}P_{H_2}^{-2.3}$.

Mahaffy and Hansen (*37*) studied ethane hydrogenolysis over an iridium film. They found that at very low partial pressures of ethane or hydrogen, the reaction order for that reactant was positive. However, as the partial pressure increased, the order decreased and eventually became negative. Using the same temperature and H_2/C_2H_6 ratios, our model predicts the same trend in the reaction orders. The same authors also found that the rate of hydrogen chemisorption is fast compared with the adsorption of ethane. Our model agrees with this as $r_1/r_2 \sim 2000$.

Förster and Otto (*27*) studied the kinetics of ethane hydrogenolysis over Co/SiO_2. They proposed a mechanism based on several assumptions. First, hydrogenation and desorption of methane fragments were assumed to be fast. Our model predicts that the hydrogenation steps (9 and 10) and the desorption of methane (step 11) are kinetically insignificant. Second, the rupture of the C–C bond was suggested to be possible only after multiple bonding to the surface, in agreement with our model. Finally, the C–C bond rupture was proposed to be irreversible. Our model predicts this step to be irreversible as well.

Using their mechanism, the authors developed a kinetic model which predicted hydrogen reaction orders in good agreement with the experimental values. By raising EH by 1.2 kcal mol^{-1} to account for possible differences in the catalysts used by Sinfelt and Förster, our model predicts hydrogen reaction orders which are in excellent agreement with the experimental values. The three sets of reaction orders are listed in Table 4. In addition, the experimental values of the activation energy were 35.1 kcal mol^{-1} for ethane hydrogenolysis and 23.7 kcal mol^{-1} for ethane adsorption. Our model predicts these values to be 34.1 kcal mol^{-1} and 17.5 kcal mol^{-1}, respectively.

CONCLUDING REMARKS

One of the objectives of the present study was to determine whether experimental data for ethane hydrogenolysis over Pt, Pd, Ir, and Co could be explained by a kinetic model based on a chemically reasonable reaction mechanism and a limited number of parameters having physical significance. We believe that we have succeeded in this respect. Specifically, we varied essentially two adjustable parameters for each metal

TABLE 4

Experimental and Predicted Hydrogen Reaction Orders for Ethane Hydrogenolysis over Cobalt

T (K)	$m_{Exp.}$	$m_{Förster}$	m_{Model}
460	−2.1	−1.8	−2.2
500	−1.7	−1.5	−1.6
556	−1.4	−1.3	−1.5

(EH and EC) and a set of four Polanyi constants (E_0) that were constrained to be approximately constant for all four metals. Furthermore, we constrained the values of EH to be near and in the same order as those values estimated by calorimetric measurements of heats of hydrogen adsorption. In addition, we constrained the values of EC to be near and in the same order as those values estimated by bond order conservation, and we similarly required the values of E_0 also to be near (i.e., within about 5 kcal/mol) those estimated by bond order conservation methods. This was accomplished without the need to adjust any preexponential factors or any values of α in the Polanyi relations.

Comment should be made about the ability to simulate the behavior of complex catalytic reaction mechanisms in terms of only a limited number of parameters. In the present case, for example, the reaction mechanism is composed of 11 steps requiring 22 kinetic rate constants. The simulations suggest, however, that steps 9–11 are kinetically insignificant, and that steps 5 and 8 occur only at a low rate (i.e., path C is insignificant). Furthermore, steps 1 and 4 are suggested to be essentially at equilibrium, while steps 6 and 7 are irreversible. Thus, of the possible 22 kinetic rate constants, at most 8 constants need be estimated: K_1, K_4, k_2, k_{-2}, k_3, k_{-3}, k_6, and k_7 (where K_i and k_i are equilibrium and rate constants for step i, respectively). Moreover, it is possible that some of these constants may occur in combinations in the rate expression, thereby reducing further the number of kinetic parameters that need be estimated. As a result, only a limited number of parameters are needed to simulate the experimental data, since only a limited number of steps in the mechanism are kinetically significant. However, the complete kinetic simulation must be carried out initially to decide which of the steps are, in fact, kinetically insignificant and may be discarded.

The above arguments lead to a further interpretation of the physical significance of the four Polanyi parameters, E_0. First, E_a refers to step 1, which is in equilibrium; therefore, the value of E_a is not kinetically significant. The parameter E_b refers to steps 3, 4, 5, 9, 10, and 11. Since steps 5–11 are not kinetically significant and step 4 is at equilibrium, the value of E_b can be identified as the Polanyi parameter for step 3. The parameter E_c is assigned to the family of reactions 6, 7, and 8. Since step 8 is not significant, the value of E_c can be identified with either step 6 or step 7, depending whether Path A or B is faster, respectively. Finally, the Polanyi parameter E_d is related by definition to step 2.

It has been documented in this study that the present kinetic model is consistent with experimental data on a variety of catalysts studied by different investigators over a wide range of experimental conditions. This does not mean that the kinetic model is correct in detail, only that it represents a majority of the experimental data that we have explored to date. Instead, the primary utility of such a kinetic model in catalysis research is to provide a framework that can be used to explain existing data from a variety of physical and chemical sources and thereby (i) predict new experiments that can be conducted to test the kinetic model and/or identify inconsistencies in existing experimental data, (ii) propose reactor operating conditions that may optimize catalytic activity or product selectivity, and (iii) suggest surface chemical properties (e.g., bond energies) that may lead to desirable catalytic performance. Importantly, as the kinetic model is revised and modified with further experimental data, it becomes a better tool for the prediction of catalyst performance in terms of catalyst surface properties.

As an example of a prediction from the present preliminary kinetic model for ethane hydrogenolysis, we show the kinetic simulations of Fig. 8. This figure shows contours of constant catalytic activity for ethane hydrogenolysis (at the reaction con-

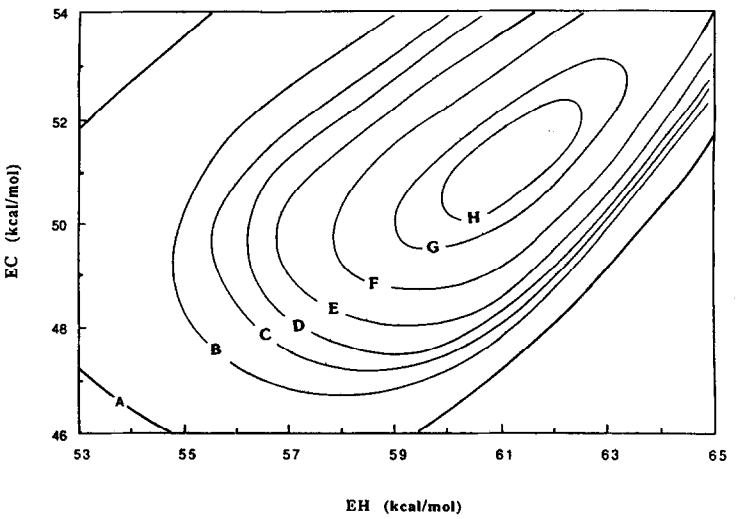

FIG. 8. Contours of constant turnover frequency (s^{-1}) for ethane hydrogenolysis versus EH and EC at 630 K, P_{H_2} = 152 Torr and $P_{C_2H_6}$ = 22.8 Torr; (A) 0.002, (B) 0.02, (C) 0.04, (D) 0.06, (E) 0.09, (F) 0.15, (G) 0.26, and (H) 0.32.

ditions typical for Pt) using different values of the surface bond energies EH and EC. Figure 8 shows, for example, that increasing the catalytic activity for hydrogenolysis can be accomplished by increasing the value of EC. Also, the catalytic activity is, in fact, very sensitive to the values of EH and EC, explaining at least partially the origin of structure sensitivity for this reaction. In particular, it may be expected that high index surface planes would bond hydrocarbon fragments more strongly than lower index surface planes, and the contours of Fig. 8 would suggest that this would lead to higher rates for ethane hydrogenolysis (as observed experimentally, Refs. *38, 39*).

ACKNOWLEDGMENTS

We thank Professor M. Boudart (Stanford) for his insight and encouragement throughout this work. We also express our thanks to D. F. Rudd and A. Trevino for their continued work in the formulation of Catalyst Design Advisory Programs.

REFERENCES

1. Dumesic, J. A., Milligan, B. A., Greppi, L. A., Balse, V. R., Sarnowski, K. T., Beall, C. E., Kataoka, T., Rudd, D. F., and Trevino, A. A., *I & EC Res.* **26,** 1399 (1987).
2. Stoltze, P., and Norskov, J. K., *J. Catal.* **110,** 1 (1988).
3. Bowker, M., Parker, I., and Waugh, K. C., *Surf. Sci. Lett.* **197,** L223 (1988).
4. Oh, S. H., Fisher, G. B., Carpenter, J. E., and Goodman, D. W., *J. Catal.* **100,** 360 (1986).
5. Dumesic, J. A., and Trevino, A. A., *J. Catal.*, in press.
6. Boudart, M., and Djéga-Mariadassou, G., "Kinetics of Heterogeneous Catalytic Reactions." Princeton Univ. Press, Princeton, NJ, 1984.
7. Sinfelt, J. H., *Catal. Rev.* **3**(2), 175 (1969).
8. Sinfelt, J. H., *Adv. Catal.* **23,** 91 (1973).
9. Shustorovich, E., *Surf. Sci.* **6,** 1 (1986).
10. Chou, P., and Vannice, M. A., *J. Catal.* **104,** 1 (1987).
11. Chou, P., and Vannice, M. A., *J. Catal.* **104,** 17 (1987).
12. Sinfelt, J. H., and Yates, D. J. C., *J. Catal.* **8,** 82 (1967).
13. Sinfelt, J. H., *J. Phys. Chem.* **68,** 344 (1964).
14. Sinfelt, J. H., and Taylor, W. F., *Trans. Faraday Soc.* **64,** 3086 (1968).
15. Cardona-Martinez, N., Ph.D. Dissertation, Univ. of Wisconsin, 1989.
16. Boudart, M., *AIChE J.* **18**(3), 465 (1972).
17. Frennet, A., Crucq, A., Degols, L., and Lienard, G., *Acta Chim. Acad. Sci. Hung.* **111**(4), 499 (1982).
18. Hermann, J. M., Gravelle-Rumeau-Maillot, M., and Gravelle, P. C., *J. Catal.* **104**(1), 136 (1987).
19. Lantz, J. B., and Gonzalez, R. D., *J. Catal.* **41,** 293 (1976).

20. Sen, B., Chou, P., and Vannice, M. A., *J. Catal.* **101**(2), 517 (1986).
21. Zowtiak, J. M., and Bartholomew, C. H., *J. Catal.* **83**(1), 107 (1983).
22. Pankratiev, Y. D., Buyanova, N. E., Turkov, V. M., Shepelin, A. P., Malyshev, E. M., and Zhdan, P. A., *React. Kinet. Catal. Lett.* **20**(1–2), 139 (1982).
23. Somorjai, G. A., "Chemistry in Two Dimensions: Surfaces." Cornell Univ. Press, London, 1981.
24. Efremov, A. A., Bakhmutova, N. I., Pankratiev, Y. D., and Kuznetsov, B. N., *React. Kinet. Catal. Lett.* **28**(1), 103 (1985).
25. Paál, Z., and Tétényi, P., *in* "Catalysis—A Specialist Periodical Report" (G. C. Bond and G. Webb, Eds.), Vol. 5, p. 80. Royal Society of Chemistry, London, 1982.
26. Tétényi, P., Guczi, L., and Sárkány, A., *Acta Chim. Acad. Sci. Hung.* **97**(2), 221 (1978).
27. Förster, H., and Otto, H. J., *Z. Phys. Chem. NF* **120,** 223 (1980).
28. Guczi, L., Frennet, A., and Ponec, V., *Acta Chim. Acad. Sci. Hung.* **112**(2), 127 (1983).
29. Gudkov, B. S., and Guczi, L., and Tétényi, P., *J. Catal.* **74,** 207 (1982).
30. Frennet, A., Degols, L., Lienard, G., and Crucq, A., *J. Catal.* **35,** 18 (1974).
31. Stuve, E. M., and Madix, R. J., *J. Phys. Chem.* **89,** 105 (1985).
32. Cimino, A., Boudart, M., and Taylor, H., *J. Phys. Chem.* **58,** 796 (1954).
33. Frennet, A., Crucq, A., Degols, L., and Lienard, G., *in* "Actas 9th Simposio Iberoamericano de Catalise, Lisbon," p. 493, 1984.
34. Sárkány, A., Guczi, L., and Tétényi, P., *Acta Chim. Acta. Sci. Hung.* **96,** 27 (1978).
35. Anderson, J. R., and Baker, B. G., *Proc. R. Soc. A* **271,** 402 (1963).
36. Foger, K., and Anderson, J. R., *J. Catal.* **59,** 325 (1979).
37. Mahaffy, P., and Hansen, R. S., *J. Chem. Phys.* **71**(4), 1853 (1979).
38. Lee, C., and Schmidt, L. D., *J. Catal.* **101,** 123 (1986).
39. Goodman, D. W., *Surf. Sci.* **123,** L679 (1982).